

Overlooked riverine contributions of dissolved neodymium and hafnium to the Amazon estuary and oceans

Received: 8 January 2023

Accepted: 3 July 2023

Published online: 12 July 2023

 Check for updatesAntao Xu¹✉, Ed Hathorne¹, Georgi Laukert^{1,2,3} & Martin Frank¹

The Amazon River accounts for 20% of global freshwater runoff and supplies vital trace metals to the Atlantic Ocean. Suspended particles within its plume are thought to partially dissolve, constituting a large potential source of metals, which is, however, not well constrained. Here we used combined neodymium (Nd) and hafnium (Hf) isotopes to disprove the release of Nd and Hf from particles as the cause of the observed dissolved concentration increases and isotopic variability across the plume. Instead, the changes reflect admixture of nearby Pará River freshwater with exceptionally high dissolved Nd and Hf concentrations contributing 45–100% of the riverine fraction to the southern and outer estuary. This result led us to develop an empirical relationship between riverine Nd concentration and pH to revise the global dissolved riverine Nd flux, which accordingly is at least three times higher than commonly used estimates. Future work should focus on contributions of low-pH rivers to global metal fluxes.

Vast amounts of nutrients, dissolved organic matter and trace metals are introduced into the Atlantic Ocean via the Amazon estuary, thereby increasing micronutrient levels¹ and enhancing productivity within the freshwater plume^{2,3}. In the Atlantic Ocean, these micronutrients allow diazotrophs and phytoplankton to flourish and sequester large amounts of atmospheric CO₂^{4,5}. The factors controlling the trace metal contents of the plume are thus crucial to constrain and include dissolved riverine inputs^{6,7}, estuarine processes (e.g., removal and addition)⁸, and the exchange between particulate and dissolved phases⁹. Despite the high dissolved riverine concentrations of trace elements and the large volume of freshwater discharged by the Amazon River ($-6.6 \times 10^{12} \text{ m}^3 \text{ yr}^{-1}$)¹⁰, sharp changes of ionic strength, temperature, and pH of the estuarine waters cause reactive metals such as iron (Fe), manganese (Mn), neodymium (Nd), or hafnium (Hf) to be removed from solution to a large extent (>50%) via salt-induced coagulation and precipitation of (nano-)particles and colloids (NPCs)^{11,12}, thereby reducing the fluxes of these metals to the Atlantic Ocean. However, inputs from diverse tributaries and suspended particle dissolution within the Amazon freshwater plume can partially compensate for the loss of rare earth elements and likely other elements in the

estuary¹³. The incomplete understanding of these processes limits the accuracy of trace element fluxes from the Amazon estuary to the Atlantic Ocean.

Radiogenic Nd and Hf isotopic compositions, expressed as ϵ_{Nd} and ϵ_{Hf} , respectively (defined by equations in Methods) are sensitive tracers of the origin and mixing of water masses^{14–16} enabled by fingerprinting of their continental source contributions with distinct isotopic signatures and their quasi-conservative behavior in seawater resulting in oceanic residence times of 300–1000 years and 250–7500 years, respectively^{17–21}. While Nd isotopes weather largely congruently, Hf isotopes are strongly affected by incongruent weathering processes^{20,22} and thus have widely been used to investigate the intensity and regimes of continental weathering and local to regional water mass mixing^{23–25}. Therefore, ϵ_{Nd} and ϵ_{Hf} are important tracers of water mixing and seawater-particle interactions in estuaries and given that rivers drain different catchments, ambient seawater and particles are often characterized by distinct isotopic fingerprints. Rousseau et al.¹³ used dissolved and particulate Nd concentrations ([Nd]) and ϵ_{Nd} signatures to investigate seawater-particle interaction processes in the Amazon estuary and observed a slight increase of dissolved [Nd] accompanied

¹GEOMAR Helmholtz Centre for Ocean Research Kiel, Kiel, Germany. ²Department of Oceanography, Dalhousie University, Halifax, NS, Canada. ³Woods Hole Oceanographic Institution, Woods Hole, MA, USA. ✉e-mail: axu@geomar.de

by a shift in ε_{Nd} to less radiogenic values at mid to high salinities. These changes led them to conclude that the dissolution of (re)suspended particles releases Nd to the river plume and that particle dissolution in estuaries is an essential source term for the global marine Nd budget, possibly affecting other elements as well. However, particle dissolution includes both the Fe–Mn oxyhydroxide and silicate phases, which likely carry different isotopic signatures that were not distinguished previously. Furthermore, potential additional sources of Nd (and Hf) were not considered, such as the adjacent Pará River, whose dissolved [Nd] and ε_{Nd} signatures were unknown but which discharges $6.6 \times 10^{11} \text{ m}^3$ of freshwater annually into the Amazon estuary²⁶.

To investigate the contributions of all potential sources to the estuary and the Atlantic Ocean, we report the isotopic compositions of dissolved Nd and Hf together with those of particulate Nd, and the concentrations of dissolved rare earth elements and yttrium ([REY]) and Hf ([Hf]) in surface waters along the entire salinity (Sal) gradient of the Amazon estuary, including the Pará River outflow (Fig. 1). Samples were obtained in April–May 2018 during RV Meteor cruise M147, which was official process study Gapr11 of the international GEOTRACES program. The ε_{Nd} and ε_{Hf} signatures reveal significant dissolved Nd and Hf inputs from the Pará River to the outer Amazon estuary, with far-reaching implications for the global marine Nd and Hf budgets and potentially also for those of other trace elements.

Results and discussion

Variability of estuarine REY and Hf concentrations

Dissolved [Nd] and [Hf] of the Pará River endmember (Sal = 0.3) are $1036 \text{ pmol kg}^{-1}$ and $13.4 \text{ pmol kg}^{-1}$, respectively, and are thus significantly higher than 502 pmol kg^{-1} and $12.3 \text{ pmol kg}^{-1}$ of the Amazon River freshwater endmember (Sal = 0.2) (Supplementary Data 1). These higher concentrations are likely a result of the overall lower pH of the Pará River pH of 6.2–7.4 (Amazon River: 6.8–7.3)²⁷ and/or feeding by tributaries from the mangrove forests, which is consistent with high trace metal export from the Amazonian mangrove forest areas^{28–30}. In addition, parent rock characteristics and floodplain supply may play a role given that elevated REY concentrations in the waters exiting the floodplain have been observed in the Amazon Basin³¹. The dissolved [Nd] of Amazon River water sampled in April–May 2018 agrees well with

the values of $471\text{--}579 \text{ pmol kg}^{-1}$ reported for August 1989³² but is substantially lower than the 850 pmol kg^{-1} found in April 2008¹³ documenting a dynamic mixing regime in the estuary and significant interannual variability, which may be related to biogeochemical changes in the floodplain³¹.

The Amazon River and Pará River freshwaters exhibit characteristic middle REY (MREY) enrichment patterns after normalization to Post-Archean Australian Shale (PAAS)^{31,33–35} (Fig. 2a–c). The REY patterns evolve towards light REY (LREY) depletion and heavy REY (HREY) enrichment signatures with increasing salinity and reach a typical seawater pattern with pronounced cerium (Ce) anomalies in the high-salinity zone (Sal > 25)³⁶ following large-scale removal of dissolved REY in the low-salinity zone (Fig. 2d, e).

Along the salinity gradient of all three transects, dissolved [Nd] and [Hf] decrease rapidly in the low-salinity zone (Sal < 6) due to the modification of the negative surface-charge of nanoparticles and colloids (NPCs) by seawater cations leading to flocculation and precipitation of river-borne NPCs^{31,37,38}. The maximum removal of 90.8% and 95.0% for Nd and 87.3% and 82.5% for Hf is observed in the north Amazon and Pará transects, respectively (Fig. 2f, g). These observations demonstrate that Hf, similar to HREY³³, is removed less efficiently than Nd during estuarine mixing, likely due to the relatively higher free Nd ion content of river water. As a net effect of competing solution- and surface-complexation processes, the proportion of Nd in the colloidal fraction is higher³³ and hence more Nd than Hf is removed by coagulation, which is also consistent with the decrease in removal efficiency from LREY to HREY during estuarine mixing^{32,39}. This is supported by recent data from the Congo River estuary, where at least 57% of the dissolved riverine Nd is removed during estuarine mixing (Sal < 23) but little or no estuarine removal of Hf has been observed based on the seasonal Congo River [Nd] and [Hf] data³⁴. In the Hudson River estuary, an increase of [Hf] at salinities between 5 and 15 has been observed, possibly related to pore water diffusion, groundwater advection or release from resuspended particles⁴⁰. To examine whether coagulation and removal of Nd and Hf continue with increasing salinity or Nd and Hf addition in the mid- to high-salinity zone occurs after initial removal, a second conservative mixing line (green dashed line in Fig. 3) was calculated between the water samples corresponding to the point of maximum removal

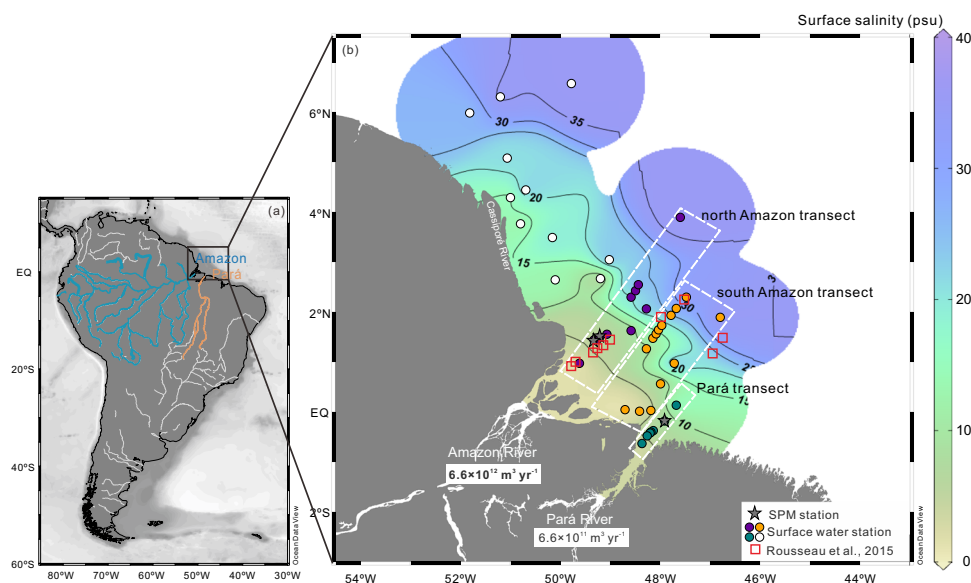


Fig. 1 Map of the study area showing sampling sites. **a** Location of study area on the North Brazil continental shelf. **b** Sampling sites in the Amazon estuary. Stars represent stations with suspended particulate matter (SPM) sampling. The three transects across the Amazon and Pará River estuaries are highlighted by differently

colored circles and dashed rectangles. Open squares show the sampling stations of Rousseau et al.¹³. The mean annual freshwater discharges of the Amazon River and Pará River are indicated^{10,26}. The map was created using Ocean Data View (<https://odv.awi.de/>)⁷⁹.

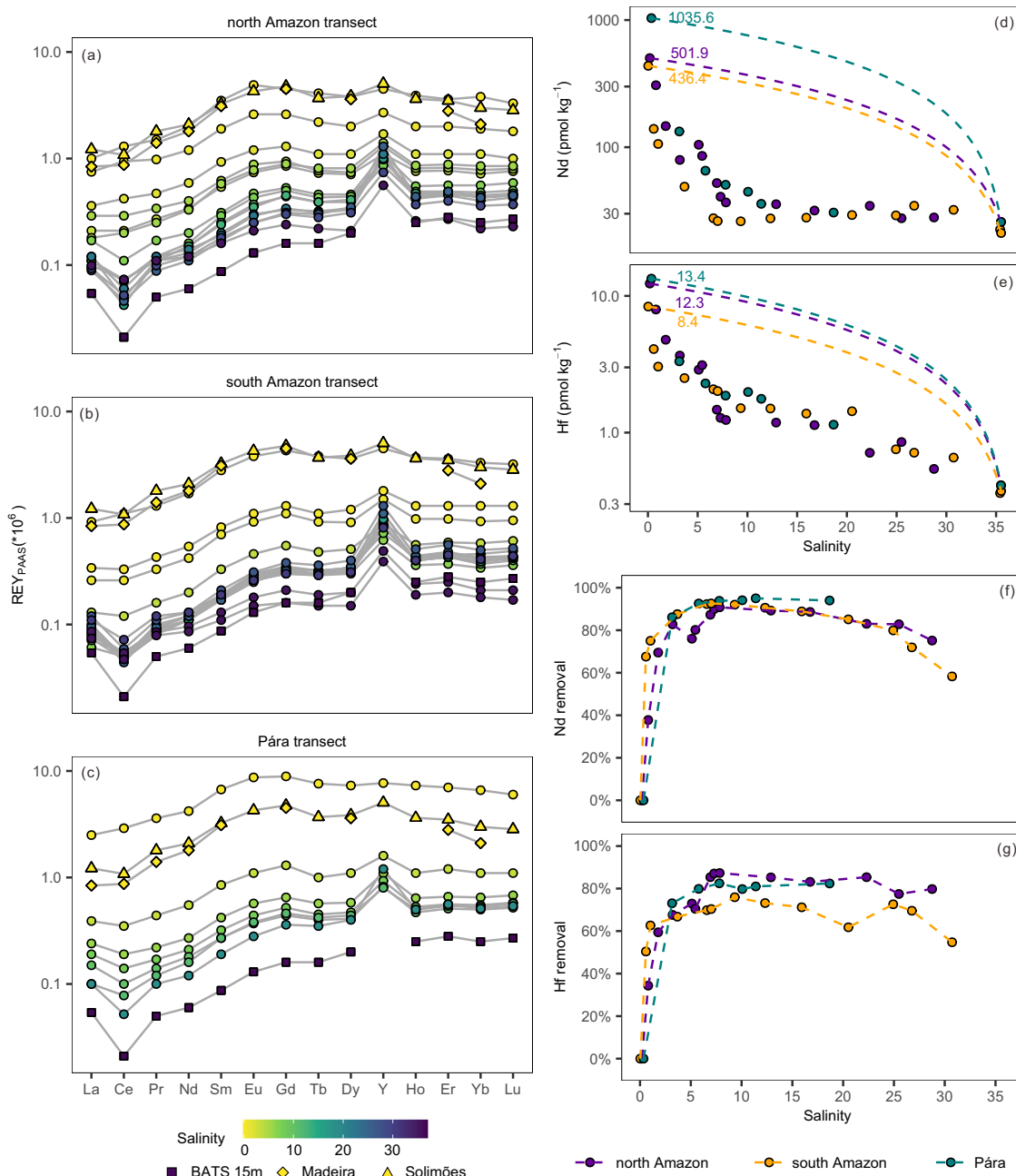


Fig. 2 | Rare earth elements and yttrium (REY) patterns and Nd and Hf concentration ([Nd], [Hf]) against salinity in surface water of the three estuarine transects. Post-Archean Australian Shale (PAAS) normalized REY patterns of surface water from the north Amazon transect (a), the south Amazon transect (b), and the Pará transect (c). Solimões river water⁴¹ and Madeira river water³¹ in the Amazon basin and BATS 15 m seawater (Sal: 36.5 psu) from the western North Atlantic²⁸ are

shown for comparison. Distributions of dissolved [Nd] (d) and [Hf] (e) of surface waters of the three estuarine transects. The dashed lines represent calculated conservative mixing lines between the freshwater (Sal = 0.2–0.3) and seawater endmembers (Sal \geq 35) in each transect. Variations in Nd and Hf removal percentage in surface water with respect to salinity (f, g), quantified using Eq. (3) in Methods. Salinity is given in psu.

percentage and the seawater endmembers. Interestingly, in the south Amazon transect, we observed elevated [Nd] and [Hf] compared to their second conservative mixing lines for salinities of 10–30 and 10–25, respectively (statistical significance $P < 0.01$ for Nd and $P = 0.06$ for Hf, t -test) (Fig. 3c, d) with a significant increase in [Nd] from 26 pmol kg⁻¹ to 35 pmol kg⁻¹, documenting the contribution of a third endmember other than Amazon River and Atlantic seawater.

ϵ_{Nd} and ϵ_{Hf} distributions across the Amazon plume

The dissolved ϵ_{Nd} and ϵ_{Hf} signatures of Amazon River freshwater are -9.4 ± 0.2 and $+1.8 \pm 0.9$, respectively, while those of Pará River freshwater are markedly less radiogenic, reaching -14.1 ± 0.2 and -4.1 ± 0.6 ,

respectively. These Pará River signatures are likely associated with higher contributions from weathering of the cratonic Shield, whose parent rock and suspended particulate matter (SPM) ϵ_{Nd} signals predominantly range from -16 to -24 ^{41–43}. The ϵ_{Nd} of the Amazon River endmember in our study agrees well with previously measured values of 9.2 ± 0.4 ⁴⁴, -8.9 ± 0.5 ⁴⁵ and -8.8 ± 0.2 ¹³. The ϵ_{Nd} values of the residual Amazon River SPM (after removal of Fe–Mn oxyhydroxides through leaching) are consistent at -11.8 ± 0.03 (± 1 standard deviation, SD, $n = 5$, open red triangles in Fig. 4a) and less radiogenic than -10.7 ¹³ or -10.3 ⁴¹ obtained for bulk SPM samples from a similar section (Fig. 1). In contrast, the ϵ_{Nd} signatures of the Fe–Mn oxyhydroxide phase of SPM that would most likely dissolve and release Nd to the plume along the north Amazon

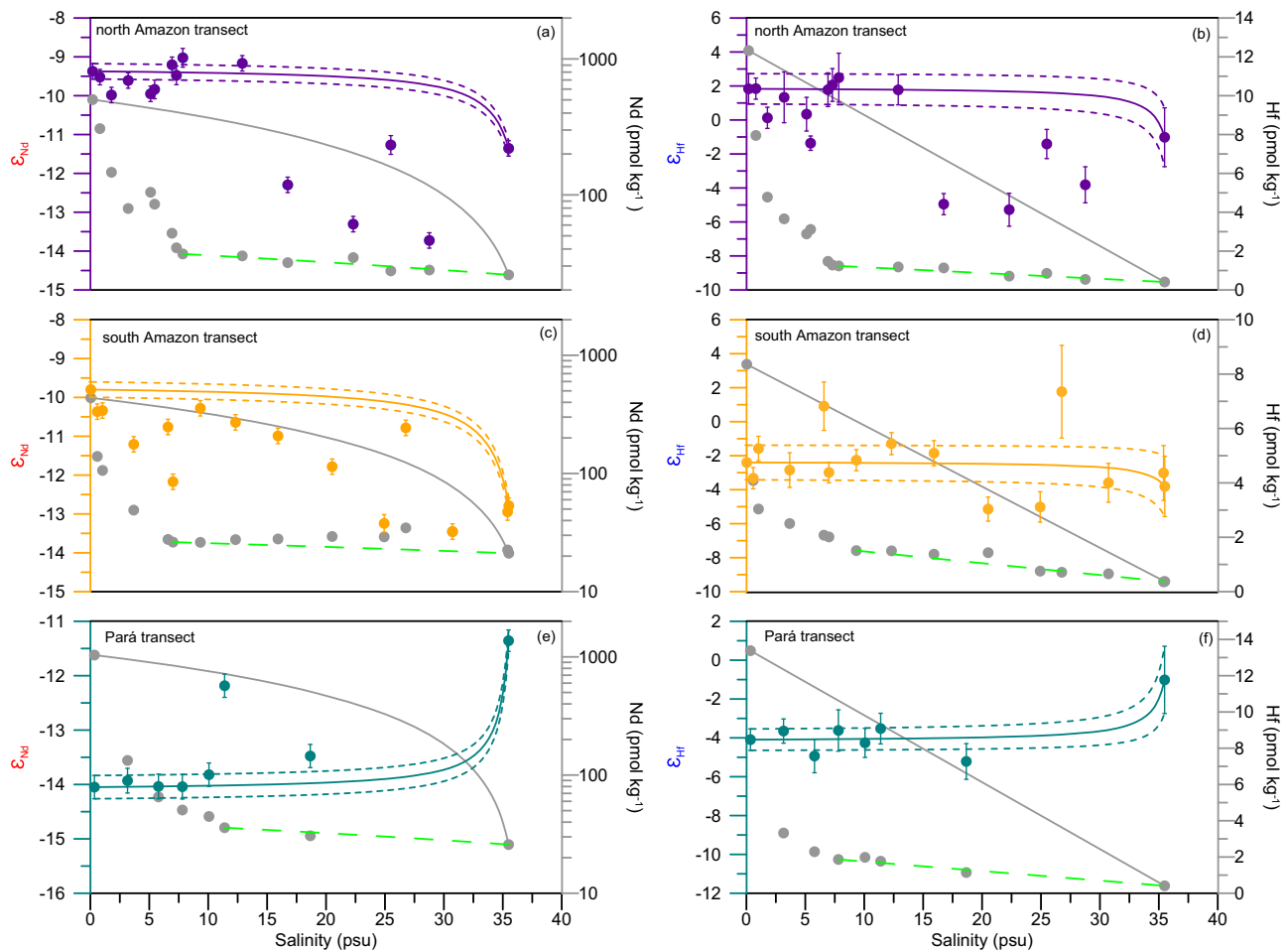


Fig. 3 | Nd and Hf isotopic composition (ϵ_{Nd} , ϵ_{Hf}) and concentration distributions along the salinity gradients of the three estuarine transects. Distributions of dissolved concentrations and isotopic compositions of Nd and Hf along the north Amazon transect (a, b), the south Amazon transect (c, d) and the Pará transect (e, f). The solid lines in each panel represent the predicted conservative mixing lines between the river water and seawater endmembers for concentrations

and isotopic compositions, respectively. The dashed lines above and below the corresponding solid lines reflect the uncertainties of the estimations of the ϵ_{Nd} and ϵ_{Hf} endmember values. Error bars correspond to the 2 standard deviations of the ϵ_{Nd} and ϵ_{Hf} measurements. The second conservative mixing line (green dashed line) for Nd and Hf is defined by water samples corresponding to the maximum removal percentage and the seawater endmembers.

transect (-8.4 ± 0.2 – -8.1 ± 0.2) (open red squares in Fig. 4a) are slightly more radiogenic and similar to the dissolved ϵ_{Nd} signature of Amazon River water. These values are also intermediate between the ϵ_{Nd} signatures of the Solimões (-7.1) and Madeira (-10.0), suggesting that the Fe–Mn oxyhydroxide fraction of SPMs sampled in the north Amazon transect mainly reflects the isotopic signals of the Amazon River that are governed by Andean tributaries⁴¹. The ϵ_{Nd} signature of Fe–Mn oxyhydroxides in the Pará transect is -10.6 ± 0.2 (open green squares in Fig. 4a) and thus less radiogenic than those of the north Amazon transect.

Figure 3 shows the evolution of ϵ_{Nd} and ϵ_{Hf} in the dissolved phase along the Amazon estuary surface salinity gradient. Throughout the low-salinity zone (Sal: 0–10) of the north Amazon and Pará transects, ϵ_{Nd} and ϵ_{Hf} values are close to the conservative mixing lines, although large amounts of dissolved Nd and Hf are clearly removed from solution, supporting the efficient removal of dissolved REY and Hf without alteration or fractionation of the radiogenic isotope signatures in the estuarine waters (Fig. 3a, b, e, f). In the mid- to high-salinity region of the south Amazon transect, where elevated dissolved [Nd] and [Hf] occur, we observe a gradual decrease in ϵ_{Nd} and ϵ_{Hf} signatures to -13.7 ± 0.2 and -5.3 ± 1.0 , respectively. Conservative mixing between the Amazon River and open Atlantic waters alone is insufficient to explain these gradients and values in the Amazon estuary, let alone the increase of dissolved [Nd] in the mid-salinity region. In previous

studies, this shift was attributed to release from sediments or suspended particles^{13,32}, but our data support an alternative explanation.

Source of elevated dissolved [Nd] and [Hf] in the Amazon estuary

The most important observation of our study is the increase in dissolved [Nd] and [Hf] at mid to high salinities accompanied by a shift to highly unradiogenic ϵ_{Nd} and ϵ_{Hf} values. This pattern could either be due to release from SPM, as suggested previously¹³, or the result of additions from other dissolved Nd and Hf sources. The labile phases of SPM are mainly Fe–Mn oxyhydroxides that tend to dissolve and release Nd to the water and are sensitive to pH and redox conditions⁴⁶. Dissolution of 0.5%–8.0% and 0.3%–5.1% of the labile Fe–Mn oxyhydroxide phases in particles from the Amazon and Pará, respectively, or partial dissolution of residual SPM (0.1%–1.1% and 0.1%–0.9%, respectively) could raise the dissolved [Nd] from the observed 26 pmol kg⁻¹ to 35 pmol kg⁻¹. However, based on our measured radiogenic Nd isotope values, the Amazon River freshwater-seawater endmember mixing combined with particle dissolution cannot account for the unradiogenic ϵ_{Nd} signatures (Fig. 4a) observed in the south Amazon transect (Supplementary Fig. 1). This is also supported by consistent REY patterns (Fig. 2b) in the south Amazon transect across the mid to high-salinity gradient of the surface estuarine waters suggesting water mass mixing without REY addition from particle release, which would result

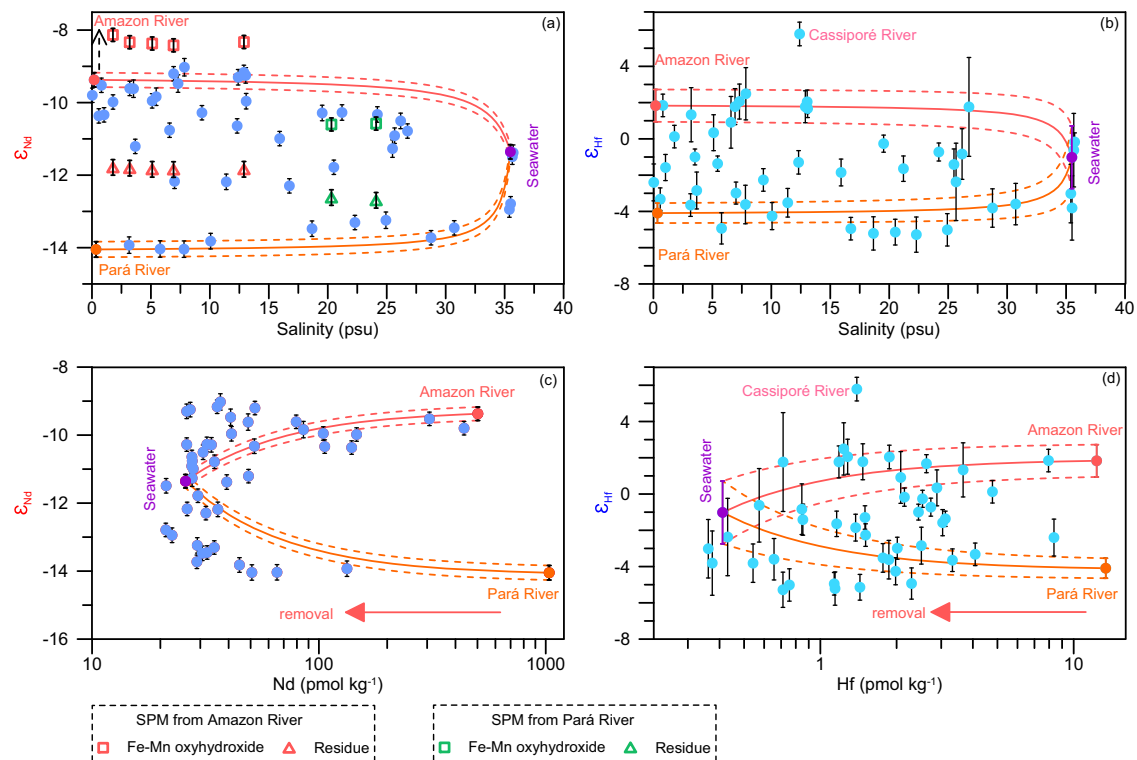


Fig. 4 | Three-endmember mixing plots of Nd and Hf isotopes (ϵ_{Nd} , ϵ_{Hf}) in the Amazon estuary. Three-endmember mixing relationships of ϵ_{Nd} (a) and ϵ_{Hf} (b) calculated based on the $^{143}Nd/^{144}Nd$ and $^{176}Hf/^{177}Hf$ ratios with corresponding Nd concentrations ([Nd]) and Hf concentrations ([Hf]) and their salinities of three dissolved sources. The open squares and triangles represent the ϵ_{Nd} signatures of the Fe–Mn oxyhydroxide fraction and of the total residual suspended particulate matter (SPM) from the Amazon River and Par  River, respectively. ϵ_{Nd} (c) and ϵ_{Hf} (d)

distributions in the Amazon estuary against [Nd] and [Hf], respectively, showing the large-scale estuarine removal of Nd and Hf. The solid lines represent conservative mixing between the freshwater and seawater endmembers. The dashed lines above and below the corresponding solid line represent uncertainties in the estimation of the ϵ_{Nd} and ϵ_{Hf} endmember values. Error bars correspond to the 2 standard deviations of the ϵ_{Nd} and ϵ_{Hf} measurements.

in flatter REY patterns with indiscernible LREY depletion (Supplementary Fig. 2). To further constrain potential sedimentary Nd and Hf sources, seven near-bottom water samples recovered in the continental shelf area of the Amazon estuary (Supplementary Fig. 3) were measured. Their mean ϵ_{Nd} and ϵ_{Hf} signatures of are -11.0 ± 1.2 (± 1 SD, $n = 7$) and 1.0 ± 1.7 (± 1 SD, $n = 7$), respectively, excluding bottom supply as a significant source of the observed unradiogenic surface water ϵ_{Nd} and ϵ_{Hf} signatures. Particle dissolution/particle-seawater interaction (i.e., boundary exchange processes) may still occur but will be restricted to the bottom layer below the freshwater plume on the continental shelf and deep-sea fan. Based on the above evidence, admixture of Par  River water, which has the highest dissolved [Nd] and [Hf] ($1036 \text{ pmol kg}^{-1}$ and $13.4 \text{ pmol kg}^{-1}$, respectively) and least radiogenic ϵ_{Nd} and ϵ_{Hf} signatures (-14.1 ± 0.2 , -4.1 ± 0.6 , respectively, Fig. 4) is the most likely explanation for the shift in isotopic signatures to highly unradiogenic values along the salinity gradient of the Amazon surface water plume. This is supported by a box model (Supplementary Figs. 4 and 5), showing that admixture of Par  River water can indeed shift the ϵ_{Nd} and ϵ_{Hf} in the outer Amazon estuary to values of -13.9 – -13.7 and -4.1 – -3.6 , respectively, which are identical within error to the measured values, indicating an additional sedimentary source is not required to explain the data. This possibility had not been considered previously because data for the Par  River were not available. Examining the spatial ϵ_{Nd} and ϵ_{Hf} distributions across the estuarine surface waters clearly reveals this impact of the Par  River on the Nd and Hf signals of the Amazon plume (Fig. 5a, b).

A three-endmember mixing model is applied to quantify the fraction of Nd and Hf added to the Amazon plume from the Par  River along the estuarine salinity gradient since the efficient removal process does not alter the ϵ_{Nd} and ϵ_{Hf} signatures. The properties of the three

major dissolved Nd endmembers (Amazon River freshwater, Par  River freshwater and Atlantic seawater) are compiled in Table 1. To compare the relative contribution of isotope signatures from the Amazon and Par  rivers, the riverine Nd and Hf proportion originating from the Par  River (named Par  riverine Nd fraction and Hf fraction) in each water sample was calculated and displayed numerically (Fig. 5c, d). In the inner Amazon River estuary (Sal < 20), the Amazon River dominates the isotope signatures of estuarine waters by supplying 55%–100% and 54%–100% riverine Nd and Hf, respectively, as indicated by more radiogenic ϵ_{Nd} and ϵ_{Hf} signatures. In contrast, the Par  River component exceeds that of the Amazon River and dominates the isotope signature of estuarine waters in the southern and outer estuary ($20 < \text{Sal} < 35$) accounting for 45%–100% and 46%–100% of the riverine Nd and Hf input, respectively. The large and previously overlooked dissolved Nd and Hf contributions from the Par  River are supported by the regional coastal circulation and satellite images of mud distribution in the estuary (Supplementary Fig. 6), as well as high concentrations of other trace metals (Fe, nickel, cobalt, titanium, aluminum, zinc, lead) in the Par  River^{27–29}. Therefore, the Par  River is an essential source of micronutrients to the Amazon estuary and to the western Atlantic and thus needs to be considered in future studies on the budget of trace elements of the western Atlantic Ocean.

Implications for global riverine dissolved Nd and Hf fluxes

Accurate oceanic budgets of Nd and Hf are needed to reliably apply Nd and Hf isotopes as tracers of water mass sources and their mixing in the modern ocean and as proxies for past changes in global ocean circulation. In the modern ocean, Hf sources have not yet been precisely constrained but include dust/particle release^{47,48}, riverine inputs^{20,34,49,50} and hydrothermal systems^{51,52}. The riverine flux of Hf to

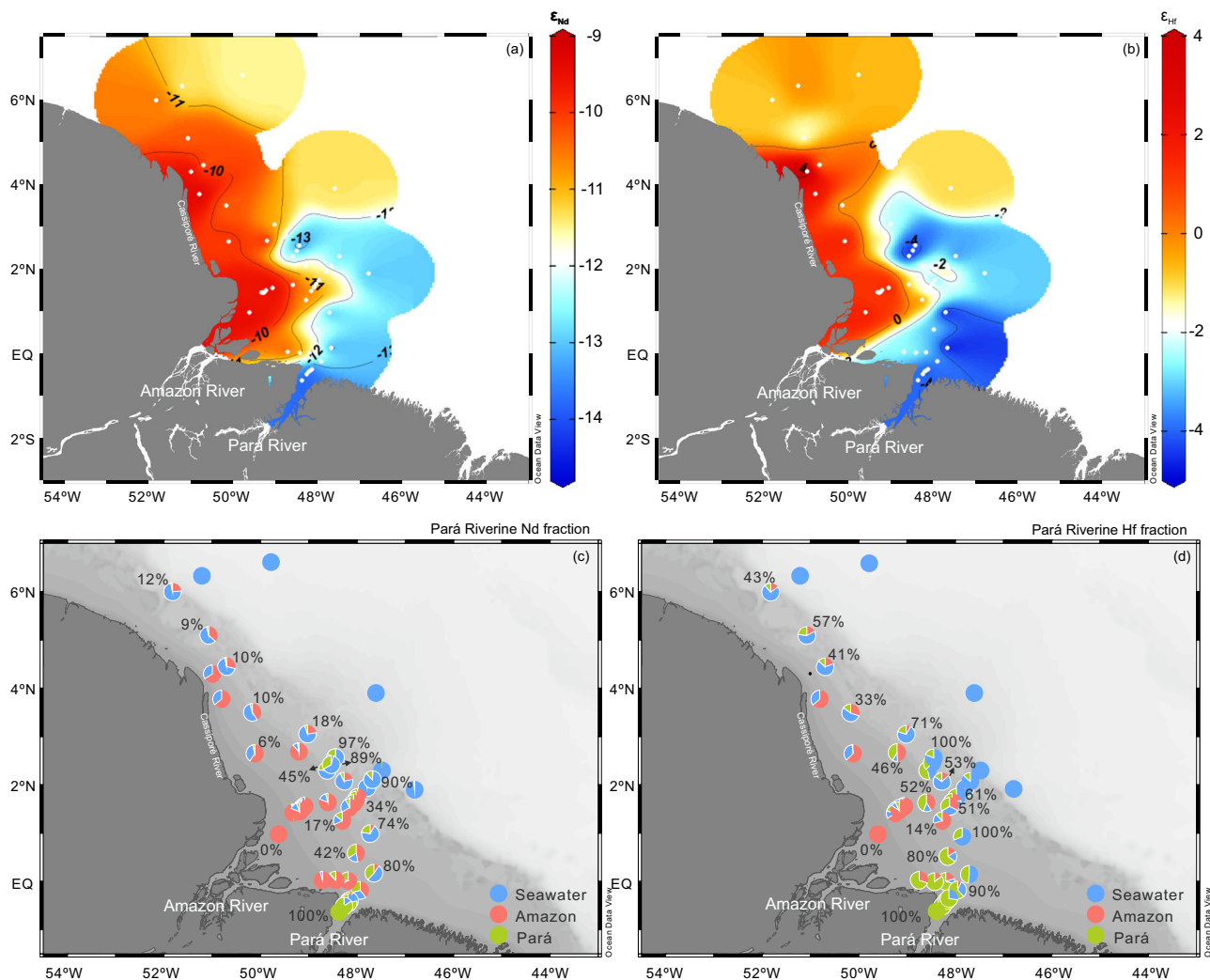


Fig. 5 | Distributions of Nd and Hf isotopes (ϵ_{Nd} , ϵ_{Hf}) and water fractions of the Pará River, the Amazon River and Atlantic seawater in the Amazon estuary. Distributions of ϵ_{Nd} (a) and ϵ_{Hf} (b) in the estuary. Pará riverine Nd fraction (c) and Hf fraction (d) defined by Eq. (8) in Methods and displayed numerically. Fractions of

Pará River water, Amazon River water and Atlantic seawater in the Amazon estuary are represented as pie charts calculated by Eqs. (4), (5), (6), and (7). Figures were produced using Ocean Data View (<https://odv.awi.de/>)⁷⁹.

Table 1 | Dissolved Nd and Hf concentrations ([Nd], [Hf]) and isotopic signatures (ϵ_{Nd} , ϵ_{Hf}) of the different endmembers

	Transect ID	Sal psu	[Nd] pmol kg ⁻¹	ϵ_{Nd}	¹⁴³ Nd/ ¹⁴⁴ Nd	[Hf] pmol kg ⁻¹	ϵ_{Hf}	¹⁷⁶ Hf/ ¹⁷⁷ Hf
Amazon River	North Amazon	0.2	501.9	-9.4	0.512158	12.3	1.8	0.282837
Pará River	Pará	0.4	1035.6	-14.1	0.511918	13.4	-4.1	0.282669
Atlantic seawater	—	35.5	25.8	-11.4	0.512056	0.4	-1.0	0.282756
Labile Fe–Mn oxyhydroxide	North Amazon	—	—	-8.3 ± 0.1	0.512211	—	—	—
	Pará	—	—	-10.6 ± 0.02	0.512094	—	—	—
Residual SPM	North Amazon	—	—	-11.8 ± 0.03	0.512031	—	—	—
	Pará	—	—	-12.7 ± 0.05	0.511987	—	—	—

The ϵ_{Nd} of Fe–Mn oxyhydroxide and residual SPM are mean values in each transect. The standard deviation for these values is calculated as the mean value over 5 and 2 samples in the north Amazon transect and the Pará transect, respectively.

the oceans is not well quantified with remarkably low [Hf] in seawater resulting in limited data availability and due to variable Hf removal during estuarine mixing^{34,40}. Therefore, it remains difficult to assess the importance of riverine Hf fluxes for the global Hf budget. There is considerably more information available on Nd inputs to the ocean via (1) dust with an estimated flux of $2 - 4 \times 10^8 \text{ g yr}^{-1} \text{ Nd}$ ^{19,21,53}, and (2) rivers

with an estimated flux of $3 - 5 \times 10^8 \text{ g yr}^{-1} \text{ Nd}$ ^{19,21}. However, the above Nd source fluxes are not sufficient to balance both [Nd] and ϵ_{Nd} distributions in the global ocean, resulting in a substantial deficit of Nd inputs of $5 - 11 \times 10^9 \text{ g yr}^{-1}$ estimated by models^{19,21,53,54}. Possible additional Nd sources include submarine groundwater discharge⁵⁵, benthic sediment fluxes⁵⁶ and release via particle dissolution¹³. However, the average

riverine [Nd] of 284 pmol kg^{-1} and 70% Nd estuarine removal, used in most models^{19,21,53–55} were calculated based on the relationship between [Nd] and the concentrations of Ca and Na across the salinity gradient in two estuaries, respectively^{57,58}. In view of higher than previously assumed [Nd] observed in our study and the low Nd removal (-57%) recently reported for the Congo River estuary³⁴ (the second largest river globally in terms of volume discharge), the flux of riverine Nd needs to be re-examined to improve our understanding of the sources of Nd in the modern ocean.

We have compiled dissolved [Nd] measurements of 49 globally distributed rivers together with their discharge and available pH values (48/49) (Supplementary Data 2) and recalculated the discharge-weighted mean dissolved riverine [Nd] ($997 \pm 36 \text{ pmol kg}^{-1}$, ± 1 standard error, SE) (see Methods) as a basis for further evaluation in a global context. A correlation between the pH of rivers and the dissolved riverine [Nd] has been noticed since the earliest studies and was attributed to solution chemistry^{6,33}. The strong inverse correlation between pH and $\log [\text{Nd}]$ ($R^2 = 0.65$, $P < 0.01$, $n = 48$, Fig. 6a) is remarkable given the likely secondary control of rock type and the amount of colloidal material in different rivers³³ and allows us to predict riverine dissolved [Nd] based on the large pH dataset available for global river waters ($n = 582$) (GEMStat^{59,60} and GLORICH⁶¹) (Supplementary Data 2). The resulting predicted weighted mean dissolved riverine [Nd] is $943 \pm 64 \text{ pmol kg}^{-1}$ ($\pm 1\text{SE}$, $n = 582$) (Fig. 6b), which is similar to the observed discharge-weighted mean river dissolved [Nd] estimated above, but more than 3–6 times the concentrations of 284 pmol kg^{-1} and 146 pmol kg^{-1} previously used in models^{19,21,53–55}. Considering a global river discharge ($133.1 \times 10^4 \text{ m}^3 \text{ s}^{-1}$)⁵⁷, a global riverine flux of $5.7 \times 10^9 \text{ g Nd yr}^{-1}$ is calculated, which is (nearly) identical to previous estimates in two studies that took the [Nd] of only 40 or 21 rivers into account (5.4 or $5.7 \times 10^9 \text{ g Nd yr}^{-1}$)^{62,63}. Using a larger global dataset ($n = 582$), our study confirms the few previous estimates of the dissolved riverine [Nd] flux while increasing data coverage by over 10-fold. The net dissolved Nd flux from rivers to the oceans is, however, controlled by the efficiency of the estuarine removal processes. A discharge-weighted mean maximum Nd removal percentage of $85 \pm 4\%$ ($\pm 1\text{SE}$, $n = 12$) is calculated from published data (12 estuarine transects) (Supplementary Data 2) (see Methods). As revealed by mixing experiments³⁸ and a lower Nd removal percentage (-50%) in the Mississippi River estuary attributed to strong aqueous complexation of REY with natural organic ligands and carbonate ions⁶⁴, we find that maximum Nd removal is closely related to dissolved organic carbon concentration ([DOC]) based on the 12 available estuarine transects. A linear correlation ($R^2 = 0.52$, $P < 0.01$) between existing observations (Fig. 6c) predicts a discharge-weighted mean maximum Nd removal percentage of $74 \pm 1\%$ ($\pm 1\text{SE}$, $n = 211$) calculated based on the discharge-weighted mean [DOC] of over 211 rivers from a larger global dataset ($n = 211$) (GEMStat^{59,60} and GLORICH⁶¹) (Fig. 6d). This result is consistent with the previously used 70% removal employed in models^{19,21,53–55}. Therefore, the revised net dissolved riverine Nd flux to the global oceans is $1.5 \times 10^9 \text{ g Nd yr}^{-1}$ (Table 2). This does not include any flux from river derived sediments as observed on continental shelves^{24,34}, but is still 3 to 5 times higher than the estimated global dust Nd input, and accounts for 17 to 27% of the global Nd input to the oceans estimated in models^{19,21,53}.

The revised global riverine dissolved Nd flux implies that this flux was previously significantly underestimated. The revised riverine Nd flux of $5.7 \times 10^9 \text{ g yr}^{-1}$ and maximum removal percentage of 74% should be implemented for models of Nd cycling in the future (Table 2). There are still many limitations related to the small available dataset of [Nd], pH values and [DOC]. Based on the existing data, riverine [DOC] seasonally variable but the scarcity of such data complicates constraining the relationship between [DOC] and the maximum Nd removal percentage. In addition, Nd removal is influenced by the content of NPCs (e.g., colloidal Fe and Mn oxides)³⁸, which cannot be estimated globally

here due to the limited available data. Therefore, more studies on rivers during both wet and dry seasons are needed to better constrain annual riverine Nd fluxes and to improve our understanding of the global Nd budget. Our findings also suggest that future work should focus on the role of rivers with low pH and high [DOC], which can contain high trace element concentrations (e.g., Fe, Mn)⁶⁵ and display low estuarine removal^{38,64}, as important sources of global trace metal fluxes to the surface oceans.

Methods

Sample collection and treatment

48 water samples along the entire salinity gradient (0 to >35) in the Amazon River estuary, the Pará River estuary and nearby regions of the Brazilian continental shelf (Fig. 1) were collected during RV Meteor cruise M147 (29 April to 20 May 2018; official process study GApr11 of the international GEOTRACES program). Surface water samples were collected either with a towed-fish or a Conductivity-Temperature-Depth (CTD) rosette equipped with 24-Niskin bottles. With the towed-fish the water samples were recovered at 2 to 3 m water depth and the bottles of the CTD rosette were closed at the same depth immediately below the surface to sample the uppermost freshwater layer. For each sample, 20 to 40 L were transferred into acid-cleaned 20 L plastic cubic containers and filtered through $0.45 \mu\text{m}$ Nucleopore filters within a few hours after collection. All samples were acidified on board to pH -2 using concentrated ultrapure distilled HCl and stored at room temperature for further treatment in the clean room laboratory at GEOMAR.

SPM samples were collected from the large amount of settled particulate material in the 20 L CTD sample plastic cubitainers of the low-salinity samples. Thus the finest fraction retained on the $0.45 \mu\text{m}$ Nucleopore filters has not been analyzed, which accounted for $3.1 \pm 1.0\%$ (1 SD, $n = 5$) of the bulk SPM sample mass calculated based on the filter weights and SPM content of SPM samples. The SPM was rinsed into smaller acid-cleaned containers using MQ water and excess water removed by siphoning after the SPM had visually settled. In the laboratory, the SPM was freeze dried at $-52 \text{ }^\circ\text{C}$ and then homogenized before further treatment.

Fe–Mn oxyhydroxide extraction and alkaline fusion

Approximately 0.2 to 1 g of SPM was treated with a diluted reductive solution consisting of 0.005 M hydroxylamine hydrochloride/1.5% acetic acid/0.03 M Na-EDTA (sodium-ethylenediaminetetraacetate) solution buffered to pH 4 with NaOH (sodium hydroxide) for 10 minutes, following Huang et al.⁶⁶ for extracting the labile Fe–Mn oxyhydroxide fraction. Total procedural blanks were below 15 pg for Nd ($n = 2$) and are hence negligible. The reproducibility was monitored by leaching marine sediment reference material MESS-2 ($n = 3$). The SPMs were then treated with strong reductive solution consisting of 0.05 M hydroxylamine hydrochloride/15% acetic acid/0.03 M Na-EDTA solution buffered to pH 4 with NaOH overnight to completely remove residual Fe–Mn oxyhydroxides, following the method applied in Gutjahr et al.⁶⁷ In this study, the labile Fe–Mn oxyhydroxide phase data we measured refers specifically to the fraction extracted by the diluted reductive solution. The residual SPM samples were dried at low temperature ($<45 \text{ }^\circ\text{C}$) in an oven and homogenized prior to alkaline fusion following Bayon et al.⁶⁸ The accuracy and reproducibility of the fusion technique was monitored by processing reference materials with each batch of SPM samples including marine sediment MESS-2 ($n = 3$), USGS reference material BHVO-2 ($n = 3$) and AGV-2 ($n = 3$). Total procedural blanks were below 80 pg for Nd ($n = 4$) are therefore negligible.

Neodymium and hafnium isotope analyses

Filtered water samples for ϵ_{Nd} and ϵ_{Hf} analysis were pre-concentrated by iron (Fe) co-precipitation. To remove most of this Fe, the samples were treated with pre-cleaned di-ethyl ether¹⁶. The REY and Hf of water

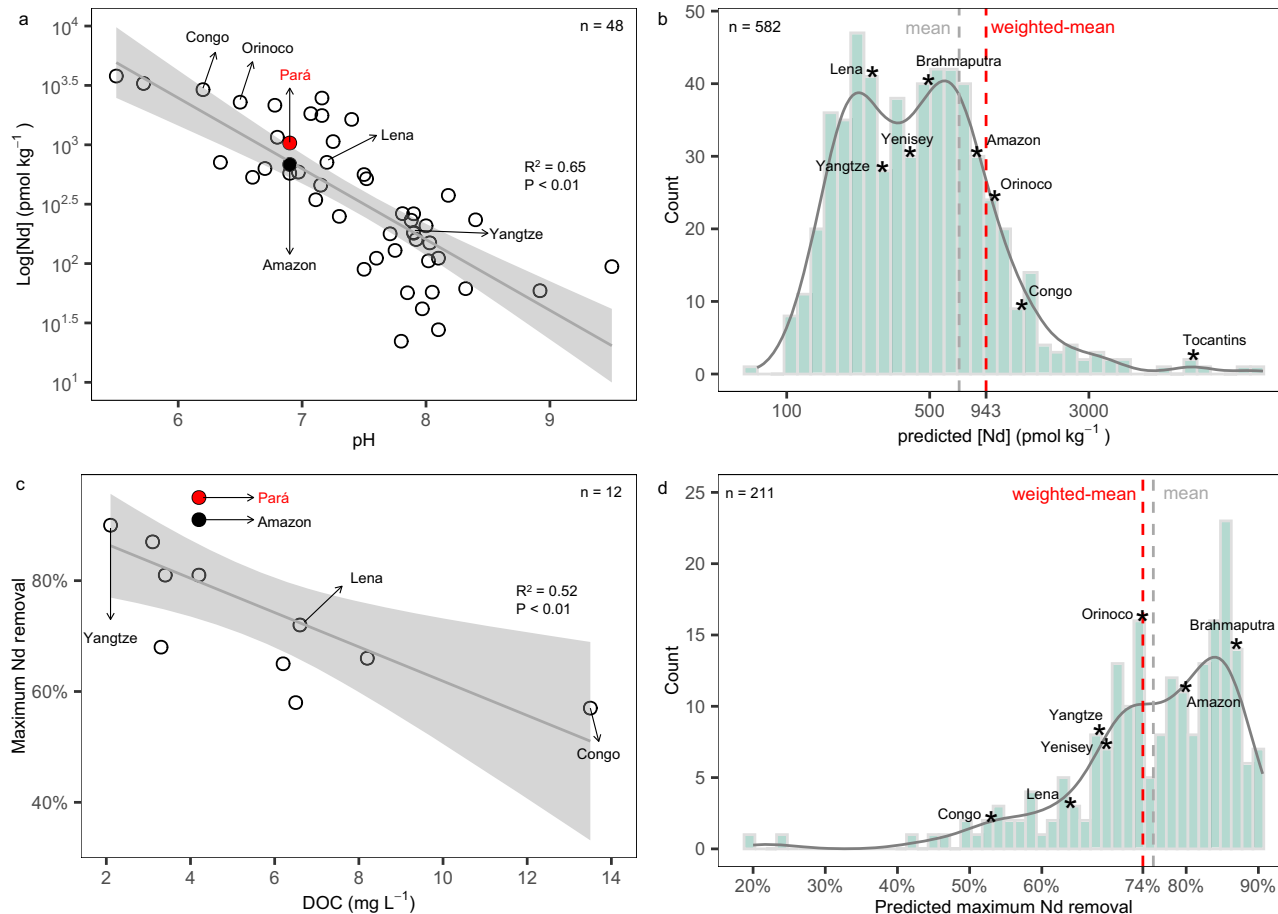


Fig. 6 | Relationships between river pH and Nd concentration ([Nd]), and between dissolved organic carbon concentration (DOC) and maximum Nd removal percentage in estuaries. a Relationship between river pH and dissolved log [Nd] calculated from 48 rivers. **b** Predicted discharge-weighted mean [Nd] based on the available global dataset ($n = 582$). **c** Relationship between [DOC] and

maximum Nd removal percentage calculated from 12 rivers. **d** Predicted discharge-weighted mean maximum Nd removal percentage based on the available global dataset ($n = 211$). Some large rivers have been flagged in panels **b** and **d** to show the impact of these highly weighted rivers on the calculations of global discharge-weighted mean [Nd] and estuarine removal percentage.

and SPM samples were separated from matrix elements using cation exchange chromatography (AG® 50W-X8, 1.4 mL, 200–400 μm) following the scheme of Stichel et al.¹⁶. Nd was further separated from the other REY for isotope measurements using Eichrom® LN-Spec resin (2 mL, 50–100 μm) following the procedure of Pin and Zalduegui⁶⁹.

Table 2 | Comparison of optimized Nd parameters between literatures and our study

	Previously used	Revised
		Weighted mean, 1SD, 1SE, 95% CI
[Nd] _{observed} (pmol kg ⁻¹)	146, 284	997, 860, 36, [927, 1067]
[Nd] _{predicted} (pmol kg ⁻¹)	—	943, 1534, 64, [818, 1067]
[Removal] _{observed} (%)	70	85, 13, 4, [78, 93]
[Removal] _{predicted} (%)	—	74, 9, 1, [73, 76]
Gross river Nd flux (g yr ⁻¹)	0.9–1.7 × 10 ⁹	5.7 × 10 ⁹
Net river Nd flux (g yr ⁻¹)	0.3–0.5 × 10 ⁹	1.5 × 10 ⁹
Global Nd budget (g yr ⁻¹)	6–9 × 10 ⁹	

Previously used [Nd]_{observed}, [Removal]_{observed}, gross, net river Nd flux and global Nd budget are based on previous studies^{19,21,53–55}. The standard deviation (1SD), standard error (1SE) and 95% confidence interval (CI) of the calculations are listed below, and a detailed uncertainty assessment is included in the Supplementary Information.

The Hf was further purified by eluting titanium (Ti) and zirconium (Zr) using Bio-Rad AG® 1-X8 resin (2 mL, 200–400 μm) following Munker et al.⁷⁰. The ¹⁴³Nd/¹⁴⁴Nd ratios were measured on a Neptune Plus MC-ICP-MS at GEOMAR and were corrected for instrumental mass bias to ¹⁴⁶Nd/¹⁴⁴Nd = 0.7219 and to ¹⁴²Nd/¹⁴⁴Nd = 1.141876 following the approach of Vance and Thirlwall⁷¹. The ¹⁴³Nd/¹⁴⁴Nd ratios of all samples were normalized to bracketing analyses of JNdI-1 standard with a value of 0.512115⁷². The ¹⁷⁶Hf/¹⁷⁷Hf ratios of the samples measured on the Neptune Plus MC-ICP-MS were corrected for instrumental mass bias to ¹⁷⁹Hf/¹⁷⁷Hf = 0.7325 applying an exponential mass fractionation law and standard JMC 475 values were within uncertainty of the accepted value of 0.28216⁷³. The total procedural laboratory blanks for water samples ($n = 6$) were negligible at <29 pg for Nd and 5–24 pg for Hf compared to sample sizes of 10–20 ng (Nd) and 2–10 ng (Hf) for isotope measurements. Secondary standard solution NIST 3135a and USGS reference material NOD-A-1 were run with water samples and USGS reference material AGV-2 and BHVO-2 were run with SPM samples to check the accuracy and external reproducibility of the procedure for Nd isotope measurements (Supplementary Data 1). For Hf isotope measurement, an internal laboratory standard solution (CGHF1, Inorganic Ventures®) and USGS reference material NOD-A-1 were measure for monitoring external reproducibility. The external reproducibility of the Nd and Hf isotope measurements of water samples was determined using standard solutions with concentrations matching those of the measured samples in the range of 0.20–0.24 ε_{Nd} units (2SD) and 0.45–2.73 ε_{Hf}

units (2 SD), respectively, while it was 0.18–0.21 ϵ_{Nd} units (2 SD) for measurements of particle samples. The 2 SD of the secondary standard NIST 3135a and CGHF1 are employed to illustrate the reproducibility of measured ϵ_{Nd} and ϵ_{Hf} in all figures and are shown in Supplementary Data 1. ϵ_{Nd} and ϵ_{Hf} are defined by the Eqs. (1) and (2), respectively:

$$\epsilon_{\text{Nd}} = \left(\frac{(143_{\text{Nd}}/144_{\text{Nd}})_{\text{sample}}}{(143_{\text{Nd}}/144_{\text{Nd}})_{\text{CHUR}}} - 1 \right) \times 10^4 \quad (1)$$

$$\epsilon_{\text{Hf}} = \left(\frac{(176_{\text{Hf}}/177_{\text{Hf}})_{\text{sample}}}{(176_{\text{Hf}}/177_{\text{Hf}})_{\text{CHUR}}} - 1 \right) \times 10^4 \quad (2)$$

where the $^{143}\text{Nd}/^{144}\text{Nd}$ and $^{176}\text{Hf}/^{177}\text{Hf}$ ratios of CHUR (Chondritic Uniform Reservoir) are 0.512638⁷⁴ and 0.282785⁷⁵, respectively.

Neodymium and hafnium concentration analyses

For Nd and Hf concentration measurements of water samples, 50 mL (low-salinity samples) to 1 L (high-salinity samples) water sample aliquots were spiked with pre-weighed ^{150}Nd and ^{180}Hf spikes, pre-concentrated using Fe co-precipitation, and purified on a AG[®] 50W-X8 column following the scheme of Rahlf et al.³⁴. Hf cuts were dissolved in 0.1 M HF for further purification using AG[®] 1-X8 resin (1.6 mL, 200–400 μm) to elute Ti, Zr and tungsten (W) following a procedure of Sahoo et al.⁷⁶. The isotope dilution measurements of the Nd and Hf concentrations based on $^{150}\text{Nd}/^{144}\text{Nd}$ and the $^{178}\text{Hf}/^{180}\text{Hf}$ ratios were carried out on a Nu Plasma MC-ICP-MS. External reproducibility (2 SD)

reproducibility and accuracy. Mean values and 2 SD for the reference material measurements are given in Supplementary Data 1.

Nd and Hf removal and three-endmember model calculations

Nd and Hf removal percentage are quantified with Eq. (3):

$$\% \text{ removal} = 1 - \frac{[\text{Nd or Hf}]_{\text{measured}}}{[\text{Nd or Hf}]_{\text{conservative}}} \times 100 \quad (3)$$

where $[\text{Nd or Hf}]_{\text{measured}}$ represents measured concentrations and $[\text{Nd or Hf}]_{\text{conservative}}$ represents concentrations expected from two-endmember conservative mixing for the same salinity. The three-endmember mixing model is established based on the $^{143}\text{Nd}/^{144}\text{Nd}$ and $^{176}\text{Hf}/^{177}\text{Hf}$ ratios with corresponding [Nd] and [Hf] and their salinities of three dissolved sources (i.e., Amazon River, Pará River and Atlantic seawater), which are listed in Table 1. Three major dissolved Nd fractions are defined: the Amazon River freshwater fraction, f_{Ama} ; the fraction from the Atlantic seawater endmember, f_{Atl} ; and the Pará River freshwater fraction, $f_{\text{Pará}}$. The fractions of f_{Ama} , f_{Atl} , $f_{\text{Pará}}$ of all samples along the estuarine gradient are listed in Supplementary Data 1 and are calculated by the Eqs. (4), (5), (6) and (7):

$$f_{\text{Ama}} + f_{\text{Pará}} + f_{\text{Atl}} = 1 \quad (4)$$

$$\text{Sal}_{\text{Ama}} \times f_{\text{Ama}} + \text{Sal}_{\text{Pará}} \times f_{\text{Pará}} + \text{Sal}_{\text{Atl}} \times f_{\text{Atl}} = \text{Sal}_{\text{sample}} \quad (5)$$

$$\frac{f_{\text{Ama}} \times [\text{Nd}]_{\text{Ama}} \times (143_{\text{Nd}}/144_{\text{Nd}})_{\text{Ama}} + f_{\text{Pará}} \times [\text{Nd}]_{\text{Pará}} \times (143_{\text{Nd}}/144_{\text{Nd}})_{\text{Pará}} + f_{\text{Atl}} \times [\text{Nd}]_{\text{Atl}} \times (143_{\text{Nd}}/144_{\text{Nd}})_{\text{Atl}}}{f_{\text{Ama}} \times [\text{Nd}]_{\text{Ama}} + f_{\text{Pará}} \times [\text{Nd}]_{\text{Pará}} + f_{\text{Atl}} \times [\text{Nd}]_{\text{Atl}}} = (143_{\text{Nd}}/144_{\text{Nd}})_{\text{sample}} \quad (6)$$

$$\frac{f_{\text{Ama}} \times [\text{Hf}]_{\text{Ama}} \times (176_{\text{Hf}}/177_{\text{Hf}})_{\text{Ama}} + f_{\text{Pará}} \times [\text{Hf}]_{\text{Pará}} \times (176_{\text{Hf}}/177_{\text{Hf}})_{\text{Pará}} + f_{\text{Atl}} \times [\text{Hf}]_{\text{Atl}} \times (176_{\text{Hf}}/177_{\text{Hf}})_{\text{Atl}}}{f_{\text{Ama}} \times [\text{Hf}]_{\text{Ama}} + f_{\text{Pará}} \times [\text{Hf}]_{\text{Pará}} + f_{\text{Atl}} \times [\text{Hf}]_{\text{Atl}}} = (176_{\text{Hf}}/177_{\text{Hf}})_{\text{sample}} \quad (7)$$

was better than 0.6% for Nd and better than 1.2% for Hf according to repeated treatment and measurement of the same sample ($n = 5$).

Rare earth elements and yttrium concentration analyses

All REY were pre-concentrated offline using a SeaFAST system (model M5 from Elemental Scientific) following a method updated from Hathorne et al.⁷⁷. Using the new system, 12 mL of acidified water sample was loaded precisely on the column using a fifth syringe pump and after the matrix was washed away, the REY were eluted with 400 μL of 1.5 M HNO_3 . Before pre-concentration, every blank, reference material and water sample (pH=2) was spiked with 12 μL of thulium solution (10 ng g^{-1}) to monitor yields, which were typically $99.9 \pm 5.9\%$ (± 1 SD, $n = 58$). Before analysis on a Thermo Element XR ICP-MS coupled with a CETAC “Aridus 2” desolvating nebulizer, all samples were diluted with 200 μL of 0.1% HNO_3 containing 10 ng g^{-1} Re as an internal standard during measurement and to account for any sample evaporation since the pre-concentration. The use of the desolvating nebulizer increases sensitivity and also decreases oxide formation, which was monitored with element solutions of barium (Ba), Ce, praseodymium (Pr) + Nd, and samarium (Sm) + europium (Eu) + gadolinium (Gd) + terbium (Tb) at the start of each analytical session. Oxide formation was generally $<0.01 \pm 0.003\%$ ($n = 3$, ± 1 SD) for Ba, $<0.05 \pm 0.01\%$ ($n = 3$, ± 1 SD) for Ce, $<0.04 \pm 0.01\%$ ($n = 3$, ± 1 SD) for Pr+Nd and $<0.04 \pm 0.13\%$ ($n = 3$, ± 1 SD) for the MREY. Certified natural river and estuarine water reference materials (NRCC SLRS-6 and SLEW-3) and GEOTRACES inter-calibration samples BATS 15 m and 2000 m⁷⁸ were pre-concentrated like the samples and measured to monitor external

The Pará riverine Nd and Hf fractions are defined by Eq. (8):

$$\text{Pará riverine Nd and Hf fraction} = \frac{f_{\text{Pará}}}{(f_{\text{Pará}} + f_{\text{Ama}})} \quad (8)$$

Discharge-weighted mean river dissolved Nd concentration and removal percentage calculations

The discharge-weighted mean dissolved [Nd] (C) of rivers was calculated by Eq. (9):

$$C = \frac{\sum_{k=1}^n D_k N_k}{\sum_{k=1}^n D_k} \quad (9)$$

where D_k is the fraction of each river discharge in the total global river discharge of $133.1 \times 10^4 \text{ m}^3 \text{ s}^{-1}$ and N_k is the [Nd] measured in each river. The discharge-weighted mean maximum estuarine Nd removal percentage (F) was calculated using Eq. (10):

$$F = \frac{\sum_{k=1}^n D_k R_k}{\sum_{k=1}^n D_k} \quad (10)$$

where D_k is as above and R_k is the Nd removal percentage calculated for each river.

Data availability

All data generated in this study are provided in the Supplementary files and are also available on PANGAEA. Global river pH and dissolved organic carbon datasets (GEMStat and GLORICH) used in this study are

available through the GEMStat website (<https://gemstat.org/>) and PANGAEA website, respectively.

References

- Rijkenberg, M. J. et al. The distribution of dissolved iron in the West Atlantic Ocean. *PLoS ONE* **9**, e101323 (2014).
- Foster, R., Subramaniam, A., Mahaffey, C., Carpenter, E., Capone, D. & Zehr, J. Influence of the Amazon River plume on distributions of free-living and symbiotic cyanobacteria in the western tropical North Atlantic Ocean. *Limnol. Oceanogr.* **52**, 517–532 (2007).
- Weber, S. C., Carpenter, E. J., Coles, V. J., Yager, P. L., Goes, J. & Montoya, J. P. Amazon River influence on nitrogen fixation and export production in the western tropical North Atlantic. *Limnol. Oceanogr.* **62**, 618–631 (2016).
- Cooley, S. R., Coles, V. J., Subramaniam, A. & Yager, P. L. Seasonal variations in the Amazon plume-related atmospheric carbon sink. *Glob. Biogeochem. Cycles* **21**, GB3014 (2007).
- Subramaniam, A. et al. Amazon River enhances diazotrophy and carbon sequestration in the tropical North Atlantic Ocean. *Proc. Natl. Acad. Sci. USA* **105**, 10460–10465 (2008).
- Goldstein, S. J. & Jacobsen, S. B. Rare earth elements in river waters. *Earth Planet. Sci. Lett.* **89**, 35–47 (1988).
- Martin, J.-M., Whitfield, M. The significance of the river input of chemical elements to the ocean. In: *Trace Metals in Sea Water* (eds Wong, C.S., Boyle, E., Bruland, K.W., Burton, J.D., Goldberg, E.D.). 265–296 (Springer US, 1983).
- Sholkovitz, E., Boyle, E. & Price, N. The removal of dissolved humic acids and iron during estuarine mixing. *Earth Planet. Sci. Lett.* **40**, 130–136 (1978).
- Lacan, F. & Jeandel, C. Neodymium isotopes as a new tool for quantifying exchange fluxes at the continent–ocean interface. *Earth Planet. Sci. Lett.* **232**, 245–257 (2005).
- Dai, A. & Trenberth, K. E. Estimates of freshwater discharge from continents: Latitudinal and seasonal variations. *J. Hydrometeorol.* **3**, 660–687 (2002).
- Boyle, E., Edmond, J. & Sholkovitz, E. The mechanism of iron removal in estuaries. *Geochim. Cosmochim. Acta* **41**, 1313–1324 (1977).
- Gledhill, M. et al. Trace metal stoichiometry of dissolved organic matter in the Amazon plume. *Sci. Adv.* **8**, eabm2249 (2022).
- Rousseau, T. C. et al. Rapid neodymium release to marine waters from lithogenic sediments in the Amazon estuary. *Nat Commun.* **6**, 7592 (2015).
- Frank, M. Radiogenic isotopes: Tracers of past ocean circulation and erosional input. *Rev. Geophys.* **40**, 1–38 (2002).
- Stichel, T. et al. Sources and input mechanisms of hafnium and neodymium in surface waters of the Atlantic sector of the Southern Ocean. *Geochim. Cosmochim. Acta* **94**, 22–37 (2012).
- Stichel, T., Frank, M., Rickli, J. & Haley, B. A. The hafnium and neodymium isotope composition of seawater in the Atlantic sector of the Southern Ocean. *Earth Planet. Sci. Lett.* **317**, 282–294 (2012).
- Firdaus, M. L., Norisuye, K., Nakagawa, Y., Nakatsuka, S. & Sohrin, Y. Dissolved and labile particulate Zr, Hf, Nb, Ta, Mo and W in the western North Pacific Ocean. *J. Oceanogr.* **64**, 247–257 (2008).
- Godfrey, L. V. et al. Hafnium and neodymium isotope variations in NE Atlantic seawater. *Geochim. Geophys. Geosyst.* **10**, Q08015 (2009).
- Rempfer, J., Stocker, T. F., Joos, F., Dutay, J.-C. & Siddall, M. Modelling Nd-isotopes with a coarse resolution ocean circulation model: sensitivities to model parameters and source/sink distributions. *Geochim. Cosmochim. Acta* **75**, 5927–5950 (2011).
- Rickli, J., Frank, M. & Halliday, A. N. The hafnium–neodymium isotopic composition of Atlantic seawater. *Earth Planet. Sci. Lett.* **280**, 118–127 (2009).
- Tachikawa, K., Athias, V. & Jeandel, C. Neodymium budget in the modern ocean and paleo-oceanographic implications. *J. Geophys. Res.* **108**, C8 (2003).
- van de Flierdt, T., Goldstein, S. L., Hemming, S. R., Roy, M., Frank, M. & Halliday, A. N. Global neodymium–hafnium isotope systematics—revisited. *Earth Planet. Sci. Lett.* **259**, 432–441 (2007).
- Gutjahr, M., Frank, M., Lippold, J. & Halliday, A. N. Peak Last Glacial weathering intensity on the North American continent recorded by the authigenic Hf isotope composition of North Atlantic deep-sea sediments. *Quat. Sci. Rev.* **99**, 97–111 (2014).
- Rickli, J., Gutjahr, M., Vance, D., Fischer-Gödde, M., Hillenbrand, C.-D. & Kuhn, G. Neodymium and hafnium boundary contributions to seawater along the West Antarctic continental margin. *Earth Planet. Sci. Lett.* **394**, 99–110 (2014).
- Filippova, A. et al. Water mass circulation and weathering inputs in the Labrador Sea based on coupled Hf–Nd isotope compositions and rare earth element distributions. *Geochim. Cosmochim. Acta* **199**, 164–184 (2017).
- Prestes, Y. O., Borba, T. A. D. C., Silva, A. C. D. & Rollnic, M. A discharge stationary model for the Pará–Amazon estuarine system. *J. Hydrol. Region. Stud.* **28**, 100668 (2020).
- Schneider, A. B., Koschinsky, A., Krause, C. H., Gledhill, M. & de Carvalho, L. M. Dynamic behavior of dissolved and soluble titanium along the salinity gradients in the Pará and Amazon estuarine system and associated plume. *Mar. Chem.* **238**, 104067 (2022).
- de Carvalho, L. M., Hollister, A. P., Trindade, C., Gledhill, M. & Koschinsky, A. Distribution and size fractionation of nickel and cobalt species along the Amazon estuary and mixing plume. *Mar. Chem.* **236**, 104019 (2021).
- Hollister, A.P., Leon, M., Scholten, J., Van Beek, P., Gledhill, M., Koschinsky, A. Distribution and flux of trace metals in the Amazon and Pará river estuary and mixing plume. *Authorea*, <https://doi.org/10.1002/essoar.10512637.10512631> (2022).
- Matos, C. R. L. et al. Seasonal changes in metal and nutrient fluxes across the sediment–water interface in tropical mangrove creeks in the Amazon region. *Appl. Geochem.* **138**, 105217 (2022).
- Barroux, G. et al. Seasonal dissolved rare earth element dynamics of the Amazon River main stem, its tributaries, and the Curuai floodplain. *Geochim. Geophys. Geosyst.* **7**, Q12005 (2006).
- Sholkovitz, E. R. The geochemistry of rare earth elements in the Amazon River estuary. *Geochim. Cosmochim. Acta* **57**, 2181–2190 (1993).
- Elderfield, H., Upstill-Goddard, R. & Sholkovitz, E. The rare earth elements in rivers, estuaries, and coastal seas and their significance to the composition of ocean waters. *Geochim. Cosmochim. Acta* **54**, 971–991 (1990).
- Rahlf, P., Laukert, G., Hathorne, E. C., Vieira, L. H. & Frank, M. Dissolved neodymium and hafnium isotopes and rare earth elements in the Congo River Plume: Tracing and quantifying continental inputs into the southeast Atlantic. *Geochim. Cosmochim. Acta* **294**, 192–214 (2021).
- Taylor SR, McLennan SM. *the Continental Crust: Its Composition and Evolution*. p. 312 (Blackwell, 1985).
- Elderfield, H. & Greaves, M. J. The rare earth elements in seawater. *Nature* **296**, 214–219 (1982).
- Hoyle, J., Elderfield, H., Gledhill, A. & Greaves, M. The behaviour of the rare earth elements during mixing of river and sea waters. *Geochim. Cosmochim. Acta* **48**, 143–149 (1984).
- Merschel, G., Bau, M. & Dantas, E. L. Contrasting impact of organic and inorganic nanoparticles and colloids on the behavior of particle-reactive elements in tropical estuaries: An experimental study. *Geochim. Cosmochim. Acta* **197**, 1–13 (2017).
- Sholkovitz, E. R. The aquatic chemistry of rare earth elements in rivers and estuaries. *Aquat. Geochem.* **1**, 1–34 (1995).

40. Godfrey, L. V., Field, M. P. & Sherrell, R. M. Estuarine distributions of Zr, Hf, and Ag in the Hudson River and the implications for their continental and anthropogenic sources to seawater. *Geochem. Geophys. Geosyst.* **9**, Q12007 (2008).
41. Merschel, G., Bau, M., Schmidt, K., Münker, C. & Dantas, E. L. Hafnium and neodymium isotopes and REY distribution in the truly dissolved, nanoparticulate/colloidal and suspended loads of rivers in the Amazon Basin, Brazil. *Geochim. Cosmochim. Acta* **213**, 383–399 (2017).
42. Höppner, N., Lucassen, F., Chiessi, C. M., Sawakuchi, A. O. & Kasemann, S. A. Holocene provenance shift of suspended particulate matter in the Amazon River basin. *Quat. Sci. Rev.* **190**, 66–80 (2018).
43. Horbe, A. M. C., Albuquerque, M. F. D. S. & Dantas, E. L. Nd and Sr isotopes and REE investigation in tropical weathering profiles of Amazon region. *Front. Earth Sci.* **10**, 845224 (2022).
44. Stordal, M. & Wasserburg, G. Neodymium isotopic study of Baffin Bay water: sources of REE from very old terranes. *Earth Planet. Sci. Lett.* **77**, 259–272 (1986).
45. Piepgras, D. & Wasserburg, G. Rare earth element transport in the western North Atlantic inferred from Nd isotopic observations. *Geochim. Cosmochim. Acta* **51**, 1257–1271 (1987).
46. Elderfield, H. & Sholkovitz, E. T. Rare earth elements in the pore waters of reducing nearshore sediments. *Earth Planet. Sci. Lett.* **82**, 280–288 (1987).
47. Rickli, J. et al. Hafnium and neodymium isotopes in surface waters of the eastern Atlantic Ocean: implications for sources and inputs of trace metals to the ocean. *Geochim. Cosmochim. Acta* **74**, 540–557 (2010).
48. Dausmann, V., Frank, M. & Zieringer, M. Water mass mixing versus local weathering inputs along the Bay of Biscay: evidence from dissolved hafnium and neodymium isotopes. *Mar. Chem.* **224**, 103844 (2020).
49. Bayon, G., Vigier, N., Burton, K. W., Jean Carignan, A. B., Etoubleau, J. & Chu, N.-C. The control of weathering processes on riverine and seawater hafnium isotope ratios. *Geology* **34**, 433–436 (2006).
50. Bayon, G. et al. Hf and Nd isotopes in marine sediments: Constraints on global silicate weathering. *Earth Planet. Sci. Lett.* **277**, 318–326 (2009).
51. Bau, M. & Koschinsky, A. Hafnium and neodymium isotopes in seawater and in ferromanganese crusts: the “element perspective”. *Earth Planet. Sci. Lett.* **241**, 952–961 (2006).
52. Godfrey, L. et al. The Hf isotopic composition of ferromanganese nodules and crusts and hydrothermal manganese deposits: Implications for seawater Hf. *Earth Planet. Sci. Lett.* **151**, 91–105 (1997).
53. Gu, S., Liu, Z., Jahn, A., Rempfer, J., Zhang, J. & Joos, F. Modeling neodymium isotopes in the ocean component of the community earth system model (CESM1). *J. Adv. Model. Earth Syst.* **11**, 624–640 (2019).
54. Arsouze, T., Dutay, J., Lacan, F. & Jeandel, C. Reconstructing the Nd oceanic cycle using a coupled dynamical-biogeochemical model. *Biogeosciences* **6**, 2829–2846 (2009).
55. Johannesson, K. H. & Burdige, D. J. Balancing the global oceanic neodymium budget: Evaluating the role of groundwater. *Earth Planet. Sci. Lett.* **253**, 129–142 (2007).
56. Abbott, A. N., Haley, B. A. & McManus, J. Bottoms up: sedimentary control of the deep North Pacific Ocean’s ϵ Nd signature. *Geology* **43**, 1035–1035 (2015).
57. Goldstein, S. J. & Jacobsen, S. B. The Nd and Sr isotopic systematics of river-water dissolved material: Implications for the sources of Nd and Sr in seawater. *Chem. Geol. Isotope Geosci. Sect.* **66**, 245–272 (1987).
58. Goldstein, S. J. & Jacobsen, S. B. REE in the Great Whale River estuary, northwest Quebec. *Earth Planet. Sci. Lett.* **88**, 241–252 (1988).
59. United Nations Environment Programme. *GEMStat database of the Global Environment Monitoring System for freshwater (GEMS/Water) Programme*. International Centre for Water Resources and Global Change K. Accessed 16-11-2020. Available upon request from GEMS/Water Data Centre: gemstat.org (International Centre for Water Resources and Global Change K, 2017).
60. Virro, H., Amatulli, G., Kmoch, A., Shen, L. & Uuema, E. GRQA: Global River Water Quality Archive. *Earth System Sci. Data* **13**, 5483–5507 (2021).
61. Hartmann, J., Lauerwald, R., Moosdorf, N. GLORICH-Global river chemistry database. *PANGAEA* <https://doi.org/10.1594/PANGAEA.902360> (2019).
62. Gaillardet, J., Viers, J., Dupré, B. Trace elements in river waters. In: *Treatise on Geochemistry* (eds. Holland, H.D., Turekian, K.K.) 225–272 (Pergamon, 2003).
63. Dang, D. H., Wang, W., Sikma, A., Chatzis, A. & Mucci, A. The contrasting estuarine geochemistry of rare earth elements between ice-covered and ice-free conditions. *Geochim. Cosmochim. Acta* **317**, 488–506 (2021).
64. Adebayo, S. B., Cui, M., Hong, T., White, C. D., Martin, E. E. & Johannesson, K. H. Rare earth elements geochemistry and Nd isotopes in the Mississippi river and gulf of Mexico mixing zone. *Front. Mar. Sci.* **5**, 166 (2018).
65. Jiann, K.-T., Santschi, P. H. & Presley, B. J. Relationships between geochemical parameters (pH, DOC, SPM, EDTA Concentrations) and trace metal (Cd, Co, Cu, Fe, Mn, Ni, Pb, Zn) concentrations in river waters of Texas (USA). *Aquat. Geochem.* **19**, 173–193 (2013).
66. Huang, H., Gutjahr, M., Kuhn, G., Hathorne, E. C. & Eisenhauer, A. Efficient extraction of past seawater Pb and Nd isotope signatures from southern ocean sediments. *Geochem. Geophys. Geosyst.* **22**, e2020GC009287 (2021).
67. Gutjahr, M., Frank, M., Stirling, C. H., Klemm, V., van de Fliedert, T. & Halliday, A. N. Reliable extraction of a deepwater trace metal isotope signal from Fe–Mn oxyhydroxide coatings of marine sediments. *Chem. Geol.* **242**, 351–370 (2007).
68. Bayon, G., Barrat, J. A., Etoubleau, J., Benoit, M., Bollinger, C. & Révillon, S. Determination of rare earth elements, Sc, Y, Zr, Ba, Hf and Th in geological samples by ICP-MS after Tm addition and alkaline fusion. *Geostand. Geoanal. Res.* **33**, 51–62 (2009).
69. Pin, C. & Zalduendi, J. S. Sequential separation of light rare-earth elements, thorium and uranium by miniaturized extraction chromatography: application to isotopic analyses of silicate rocks. *Anal. Chim. Acta* **339**, 79–89 (1997).
70. Münker, C., Weyer, S., Scherer, E. & Mezger, K. Separation of high field strength elements (Nb, Ta, Zr, Hf) and Lu from rock samples for MC-ICPMS measurements. *Geochem. Geophys. Geosyst.* **2**, 2001GC000183 (2001).
71. Vance, D. & Thirlwall, M. An assessment of mass discrimination in MC-ICPMS using Nd isotopes. *Chem. Geol.* **185**, 227–240 (2002).
72. Tanaka, T. et al. JNd1-1: a neodymium isotopic reference in consistency with LaJolla neodymium. *Chem. Geol.* **168**, 279–281 (2000).
73. Nowell, G. et al. High precision Hf isotope measurements of MORB and OIB by thermal ionisation mass spectrometry: insights into the depleted mantle. *Chem. Geol.* **149**, 211–233 (1998).
74. Jacobsen, S. B. & Wasserburg, G. Sm–Nd isotopic evolution of chondrites. *Earth Planet. Sci. Lett.* **50**, 139–155 (1980).
75. Bouvier, A., Vervoort, J. D. & Patchett, P. J. The Lu–Hf and Sm–Nd isotopic composition of CHUR: Constraints from unequilibrated chondrites and implications for the bulk composition of terrestrial planets. *Earth Planet. Sci. Lett.* **273**, 48–57 (2008).
76. Sahoo, Y. V., Nakai, S. & Ali, A. Modified ion exchange separation for tungsten isotopic measurements from kimberlite samples using multi-collector inductively coupled plasma mass spectrometry. *Analyst* **131**, 434–439 (2006).

77. Hathorne, E. C., Haley, B., Stichel, T., Grasse, P., Zieringer, M. & Frank, M. Online preconcentration ICP-MS analysis of rare earth elements in seawater. *Geochem. Geophys. Geosyst.* **13**, Q01020 (2012).
78. van de Flierdt, T. et al. GEOTRACES intercalibration of neodymium isotopes and rare earth element concentrations in seawater and suspended particles. Part 1: reproducibility of results for the international intercomparison. *Limnol. Oceanogr. Methods* **10**, 234–251 (2012).
79. Schlitzer, R. *Ocean Data View*. <https://odv.awi.de/> (2020).

Acknowledgements

We thank Andrea Koschinsky, the captain and crew of RV Meteor for their help and support during cruise M147. We also thank Jutta Heinze, Sieglinde Kolbrink, Marcus Gutjahr and Christopher Siebert for laboratory support and Lisa Bretschneider for sampling as well as Te Liu and Jörg Rickli for helpful discussions. We thank Carlos Eduardo de Rezende for the suspended matter concentration data. We also acknowledge Tristan C.C. Rousseau and Jeroen E. Sonke for their valuable advice on the mixing calculations. The China Scholarship Council (CSC) is acknowledged for financial support of A.X. during this study. G.L. gratefully acknowledges financial support from the Ocean Frontier Institute under a Canada First Research Excellence Fund award.

Author contributions

A.X., M.F., and E.H. designed and coordinated the study. M.F. and E.H. conducted the sampling. A.X. carried out the analytical work with guidance from E.H. and G.L. A.X. wrote the manuscript. All coauthors contributed to the final version.

Funding

Open Access funding enabled and organized by Projekt DEAL.

Competing interests

The authors declare no competing interests.

Additional information

Supplementary information The online version contains supplementary material available at <https://doi.org/10.1038/s41467-023-39922-3>.

Correspondence and requests for materials should be addressed to Antao Xu.

Peer review information *Nature Communications* thanks Jeremie Garnier and Alan Shiller for their contribution to the peer review of this work. A peer review file is available.

Reprints and permissions information is available at <http://www.nature.com/reprints>

Publisher's note Springer Nature remains neutral with regard to jurisdictional claims in published maps and institutional affiliations.

Open Access This article is licensed under a Creative Commons Attribution 4.0 International License, which permits use, sharing, adaptation, distribution and reproduction in any medium or format, as long as you give appropriate credit to the original author(s) and the source, provide a link to the Creative Commons license, and indicate if changes were made. The images or other third party material in this article are included in the article's Creative Commons license, unless indicated otherwise in a credit line to the material. If material is not included in the article's Creative Commons license and your intended use is not permitted by statutory regulation or exceeds the permitted use, you will need to obtain permission directly from the copyright holder. To view a copy of this license, visit <http://creativecommons.org/licenses/by/4.0/>.

© The Author(s) 2023